A semi-explicit algorithm for solving multibody contact dynamics with large deformation

Lei Peng, Zhi-Qiang Feng, Pierre Joli

A semi-explicit algorithm for solving multibody contact dynamics with large deformation

Lei Peng [a,b], Zhi-Qiang Feng [a,b,*], Pierre Joli [b]

[a] *School of Mechanics and Engineering, Southwest Jiaotong University, Chengdu, China*

[b] *LMEE Univ-Evry, Université Paris-Saclay, Evry, France*

Abstract

This work is devoted to the numerical modeling of contact problems in the context of multibody dynamics. Non-linearities including large deformation and frictional contact are modeled based on the finite element method. An improved approach by means of a semi-explicit calculation is applied to integrate the equation of motion. The frictional contact forces and the relative velocity establish an implicit relationship within the bi-potential framework. A hybrid methodology consisting of the Octree structure and the bounding volume hierarchy is proposed to reduce exhaustive contact inspections. Two numerical examples implemented in our in-house finite element software FER/Impact are given to illustrate the efficiency and accuracy of the resulting methods.

Key words: Semi-explicit algorithm, Contact detection, Multibody dynamics, Large deformation, Bi-potential method.

1 Introduction

Impact and friction phenomenons play a noticeable role in multibody contact dynamics. These phenomenons are very complex and usually difficult to be modeled because multiple nonlinearities are involved. Besides, variables like velocity, acceleration show sudden changes and discontinuity in a very short duration. For the early studies, multibody systems were mostly analyzed by

* Corresponding author. Tel.: +33(0)169477501. *E-mail address*: zhiqiang.feng@univ-evry.fr (ZQ Feng)

using rigid bodies or elastic bodies. With the practical problems growing larger and more complicated, the study on the multibody contact dynamics dealing with very soft materials has received a special attention, for example, the soft textile composite reinforcements [1] and the biomechanical system [2,3].

In the aspects of solving dynamic contact/impact problems, the existing approaches can be distinguished with two major branches. One is the impulse-momentum method, which analyzes the impact process in two intervals, namely before and after impact. To reduce the complexity of the actual physical process of impact, this method usually assumes the impact duration as an instantaneous process, and the configuration of interacting bodies remains unchanged. The cases of analyzing impact between rigid bodies or linear flexible bodies by using impulse-momentum methods have been extensively studied in the references [4–7]. However, the extension to large deformation, in particular with sustained contact and friction problems remains a difficult task. Another one is the so called force-based method, which calculates the contact force based on the contact constraints. These kind of approaches treat the contact force in a continuous manner, and require no assumptions to model the mechanical behavior of multiple contacts. In the literature, most proposed force-based approaches can be divided between the penalty method [8–10] and the multiplier Lagrangian method [11–14]. The accuracy of the penalty method strongly depends on the penalty parameter, however, no clear rules are presented to choose this parameter. Furthermore, this method can not satisfy accurately the friction laws. The multiplier Lagrangian method can enforce the zero-penetration condition exactly by introducing a set of multipliers representing contact forces. Nevertheless, both the generalized coordinates and multipliers are unknown values, thus leading to an increase in the size of equation systems.

De Saxcé and Feng [15] have proposed the bi-potential method, in which a formulation extended by the augmented Lagrangian method is provided. This method can make certain mathematical reduction by using a unique mathematical projection operator that does not increase the unknown of Lagrangian multipliers. At the same time, contact forces can be accurately obtained by considering dissipative constitutive contact laws such as Coulomb frictional law. In the work of Feng et al [16,17], a first-order implicit scheme is suggested to deal with impact systems composing of two or three interacting bodies. This scheme is unconditionally stable and capable of calculating solutions using larger increments. Nevertheless, the stability comes at a cost of assembling the stiffness matrix and checking convergence at each time step, which is not applicable for more complicated problems with large data systems. In this paper, we extend the current work in order to include multibody contact dynamics and large deformation. A semi-explicit method within the bi-potential framework is proposed to integrate the equations of motion. In particular, the unilateral contact constraints are enforced via a reaction-

velocity formulation. This method can highly reduce the computational cost while not sacrificing numerical stability. Because the unilateral contact and frictional non-linearities are separated rather than being considered at the same time. Furthermore, the contact forces are solved in an implicit manner, and no construction and no factorization of global stiffness matrix are required at each time step.

Unlike simple cases of handling very few interacting bodies, the contact detection for multibody systems can be much more complicated. For one thing, bodies within the scene can move and deform unpredicted for the precious step. For another thing, high frequently occurrence of contact events can significantly increase the computational cost. In the literature, the range of contact detection algorithms proposed for the finite element modeling is various. These include methods based on the slave-master surface [18], the nested bucket [19], the sweep and prune [20], the closest features [21–23], LC-grid [24], etc. For survey articles on contact detection, the reader is referred to [25,26]. In this work, we present a three-stages methodology gathering from computer science to accelerate contact detection. At the first stage, a tree structure based on Octrees is used to find the initial pairs of objects that are possible to come into contact in multibody systems. A second stage consists of performing an elementary test on a optimal hierarchies of axis-aligned bounding boxes (AABBs). More specifically, these AABBs are separately assigned by specific geometrical components to eliminate duplicate elementary tests that arise in face-face intersections. The final stage of the detection level utilizes thorough checks for actual contact, in which an optimization approach is applied to compute the minimum distance from slave nodes to master finite elements.

The article is organized as follows: in Section 2, the description of contact kinematics is formulated. The finite element formulations of hyperelastic materials and the calculation of internal forces are given in Section 3. The bi-potential method and the semi-explicit algorithm to solve multibody dynamics are provided in Section 4. Section 5 outlines the proposed three-level approach for the contact detection. Section 6 presents two numerical examples. In Section 7, a few concluding remarks are drawn.

2 Contact kinematics

First of all, some basic definitions and notations are set up. Let β^1 and β^2 be two bodies in frictional contact (Figure 1). The surface of the bodies is defined as $\Gamma^i = \partial\beta^i, i \in \{1, 2\}$, which includes three parts: Dirichlet boundary Γ^i_u with prescribed displacements $\mathbf{u}_i$, Neumann boundary Γ^i_t with prescribed tractions $\bar{\mathbf{t}}_i$, and the potential contact surface Γ^i_c. It is required that these boundaries should fulfill $\Gamma^i_u \cup \Gamma^i_t \cup \Gamma^i_c = \Gamma^i$, and $\Gamma^i_u \cap \Gamma^i_t = \Gamma^i_t \cap \Gamma^i_c = \Gamma^i_u \cap \Gamma^i_c = \emptyset$

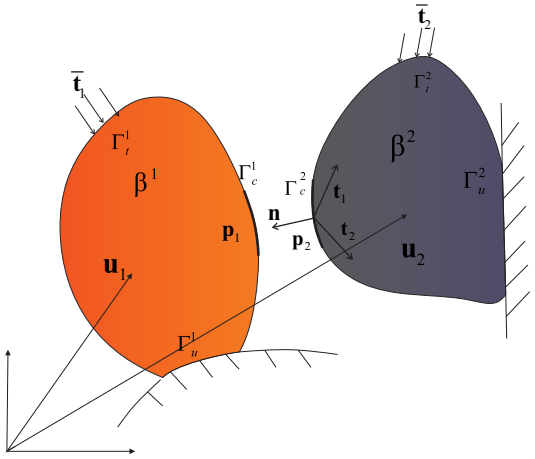

Fig. 1. Contact kinematics

Let us consider a set of contacting points $\mathbf{p}_2^\alpha$ ($\alpha = 1...N_c$) on surface Γ_c^2. The orthogonal projection of $\mathbf{p}_2^\alpha$ on Γ_c^1 is defined by $\mathbf{p}_1^\alpha$. For each contact α, the relative distance vector can be represented by:

$$\mathbf{x}^\alpha = \mathbf{u}(\mathbf{p}_2^\alpha) - \mathbf{u}(\mathbf{p}_1^\alpha) = \mathbf{B}_2^\alpha \mathbf{u}_2 - \mathbf{B}_1^\alpha \mathbf{u}_1 \tag{1}$$

where $\mathbf{B}_1^\alpha$ (resp. $\mathbf{B}_2^\alpha$) denotes the interpolation matrix derived from the adjacent nodes. Note that every point $\mathbf{p}_1^\alpha$ on Γ_c^1 can be written by $\mathbf{u}(\mathbf{p}_1^\alpha) = \mathbf{u}_1^\alpha(\varepsilon, \eta)$, where (ε, η) denotes the parameterization of the boundary Γ_c^1, see Laursen and Simo [27].

Eq.(1) can be written in the form of displacement mapping functions as:

$$\mathbf{x}^\alpha = \hbar^\alpha(\mathbf{u_2}) - \hbar^\alpha(\mathbf{u_1}) \tag{2}$$

If we define $\mathbf{H}^\alpha(\mathbf{u}) = \frac{\partial \hbar^\alpha(\mathbf{u})}{\partial \mathbf{u}}$, at time t, we obtain:

$$\dot{\mathbf{x}}^\alpha(t) = \mathbf{H}^\alpha(\mathbf{u}_2)\dot{\mathbf{u}}_2(t) - \mathbf{H}^\alpha(\mathbf{u}_1)\dot{\mathbf{u}}_1(t) \tag{3}$$

or

$$\begin{aligned} \dot{\mathbf{x}}^\alpha(\mathbf{t}) &= [\mathbf{H}^\alpha(\mathbf{u}_2), -\mathbf{H}^\alpha(\mathbf{u}_1)] \left\{ \begin{array}{c} \dot{\mathbf{u}}_2(t) \\ \dot{\mathbf{u}}_1(t) \end{array} \right\} \\ &= \mathbf{H}^\alpha \dot{\mathbf{u}}(t) \end{aligned} \tag{4}$$

where $\mathbf{H}^\alpha$ is linear at each time step.

Let $\mathbf{r}^\alpha$ be the contact force distribution exerted on β^1 at $\mathbf{p}_2^\alpha$ from β^2. According to the action-reaction principle, β^2 is subjected to the stress $-\mathbf{r}^\alpha$. Thus, the

dual relation for contact forces can be represented as:

$$\mathbf{R}_1 = \mathbf{H}^\alpha(\mathbf{u}_1)^T\mathbf{r}^\alpha,\ \mathbf{R}_2 = -\mathbf{H}^\alpha(\mathbf{u}_2)^T\mathbf{r}^\alpha \tag{5}$$

and

$$\mathbf{R}^\alpha = \begin{Bmatrix} \mathbf{R}_1 \\ \mathbf{R}_2 \end{Bmatrix} = (\mathbf{H}^\alpha)^T\mathbf{r}^\alpha \tag{6}$$

where $\mathbf{R}^\alpha$ is the contact forces in the global system frame.

From the transformation matrices for each object $\mathbf{H}^\alpha(\mathbf{u})$, we can have the following complementary notations:

$$\mathbf{H} = \begin{bmatrix} \mathbf{H}_1 \\ \vdots \\ \mathbf{H}_{N_c} \end{bmatrix}, \dot{\mathbf{x}} = \begin{Bmatrix} \dot{\mathbf{x}}_1 \\ \vdots \\ \dot{\mathbf{x}}_{Nc} \end{Bmatrix}, \mathbf{r} = \begin{Bmatrix} \mathbf{r}_1 \\ \vdots \\ \mathbf{r}_{Nc} \end{Bmatrix} \tag{7}$$

and

$$\mathbf{R} = \sum_{\alpha=1}^{Nc} \mathbf{R}^\alpha = \mathbf{H}^T\mathbf{r} \tag{8}$$

$$\dot{\mathbf{x}} = \mathbf{H}\dot{\mathbf{u}} \tag{9}$$

On the contact surface, a unique normal $\mathbf{n}$ is defined, and the tangential plane orthogonal to $\mathbf{n}$ is donated as $\mathbf{t}$. In the local reference frame defined by $\mathbf{n}$ and $\mathbf{t}$, any velocity vector $\dot{\mathbf{x}}$ and the contact traction $\mathbf{r}$ can be decomposed as:

$$\dot{\mathbf{x}} = \dot{\mathbf{x}}_t + \dot{x}_n\mathbf{n}, \quad \mathbf{r} = \mathbf{r}_t + r_n\mathbf{n} \tag{10}$$

2.1 Signorini law and Coulomb friction rule

Impenetrability is a main feature of unilateral contact, which implies that the contact points are not allowed to cross the boundaries of antagonist bodies. As a consequence, the relative distance x_n and reaction force r_n between contacting bodies are characterized to be non-negative, so that $x_n \geq 0$, $r_n \geq 0$. Moreover, the reaction force vanishes if contact points are not strictly in contact: $x_n > 0 \Rightarrow r_n = 0$. This set of relations are known as the Signorini law, which may be summarized in the following complementary equations:

$$\text{Signorini}(x_n, r_n) \Leftrightarrow x_n \geq 0\,, \quad r_n \geq 0\,, \quad x_n\, r_n = 0\,. \tag{11}$$

For dynamic contact analysis, the potential contact surfaces Γ_c^1 can be separated into two parts: ${}^+\Gamma_c^1$ where the body is in contact with Γ_c^2 and ${}^-\Gamma_c^1$ where the body is separated from Γ_c^2. Generally, The unilateral condition Eq.(11) can be formulated in a rate form by relative velocity:

$$\text{Signorini}(\dot{x}_n\, r_n) \Leftrightarrow \dot{x}_n \geq 0\,, \quad r_n \geq 0\,, \quad \dot{x}_n\, r_n = 0 \qquad \text{on } {}^+\Gamma_c^1\,. \tag{12}$$

The bodies are separating when $\dot{x}_n > 0$ and remain in contact for $\dot{x}_n = 0$.

A rate-independent dry-friction law is broadly based on a kinematic slip law. Consequently, the classic Coulomb friction rule can be adopted to relate the sliding velocity $\dot{\mathbf{x}}_\mathbf{t}$ and the friction force $\mathbf{r}_t$. In this rule, the friction force lies in the Coulomb's convex cone K_μ: $|\mathbf{r}_t\| \leq \mu r_n$, μ is the coefficient of friction. When the sliding velocity is not equal to zero, the friction force is opposite to the velocity: $||\dot{\mathbf{x}}_t|| \neq 0 \Rightarrow \mathbf{r_t} = -\mu r_\mathbf{n} \frac{\dot{\mathbf{x}}_\mathbf{t}}{||\dot{\mathbf{x}}_\mathbf{t}||}$. These two conditions are stated as:

$$\text{Coulomb}(\dot{\mathbf{x}}_t,\mathbf{r}_t) \Leftrightarrow \text{if } ||\dot{\mathbf{x}}_\mathrm{t}|| = 0 \text{ then } ||\mathbf{r}_\mathrm{t}|| - \mu \mathrm{r_n} \leq 0 \text{ else } \mathbf{r}_\mathrm{t} = -\mu \mathrm{r_n} \frac{\dot{\mathbf{x}}_\mathrm{t}}{||\dot{\mathbf{x}}_\mathrm{t}||} \tag{13}$$

or equivalent to

$$\text{Coulomb}(\dot{\mathbf{x}}_t,\mathbf{r}_t) \Leftrightarrow \vartheta = ||\mathbf{r}_t|| - \mu r_n \leq 0, \quad \dot{\mathbf{x}}_t = -\lambda \frac{\mathbf{r}_t}{||\mathbf{r}_t||}, \quad \lambda \geq 0, \quad \vartheta\lambda = 0 \tag{14}$$

On the contact surface ${}^+\Gamma_c^1$, the sliding rule can be combined with the rate form of the Signorini conditions to obtain the frictional contact law. This complete law specifies possible scenarios on the contact area, which is thus a complex non-smooth dissipative law including three statuses:

$$\begin{array}{lll} \text{if} & r_n = 0 \quad \text{then} \quad \dot{x}_n \geq 0 & \text{separating} \\ \text{elseif} & \mathbf{r} \in \text{int} K_\mu \quad \text{then} \quad \dot{x}_n = 0 \text{ and } \dot{\mathbf{x}}_t = \mathbf{0} & \text{sticking} \\ \text{else} & \left\{ \begin{array}{l} (\mathbf{r} \in \text{bd} K_\mu \text{ and } \quad r_n > 0), \\ \left\{ x_n = 0 \quad \text{and} \quad \exists \lambda > 0 \quad \text{such that} \quad -\dot{\mathbf{x}}_t = \dot{\lambda} \frac{\mathbf{r}_t}{||\mathbf{r}_t||} \right. \end{array} \right. & \text{sliding} \end{array} \tag{15}$$

where "int K_μ" and "bd K_μ" denote the interior and the boundary of K_μ, respectively.

3 Variational equations and calculation of internal forces

For dynamic multibody contact problems involving large deformations, the nonlinear relation between strains and displacements cannot be ignored. The

Green-Lagrange strain tensor $\mathbf{E}$ can be written with linear and nonlinear items in function of nodal displacement as follows

$$\mathbf{E} = \left(\mathbf{B}_L + \frac{1}{2}\mathbf{B}_{NL}(\mathbf{u})\right)\mathbf{u} \tag{16}$$

where $\mathbf{B}_L$ is the matrix which relates the linear strain term to the nodal displacements, and $\mathbf{B}_{NL}$ relates the nonlinear strain to the nodal displacements. $\mathbf{u}$ the displacement vector. The incremental of Eq.(16) is given:

$$\delta\mathbf{E} = (\mathbf{B}_L + \mathbf{B}_{NL}(\mathbf{u}))\delta\mathbf{u}. \tag{17}$$

The constraint of incompressibility (isochoric deformation) is given by

$$J = \det(\mathbf{F}), \quad \mathbf{F} = \mathbf{1} + \nabla\mathbf{u} \tag{18}$$

where $\mathbf{F}$ donates deformation gradient, and $\mathbf{C}$ represent the stretch tensor or the right Cauchy-Green strain tensor ($\mathbf{C} = \mathbf{F}^T\mathbf{F}^T$).

In the case of hyperelastic law, there exists an elastic potential function W(or strain energy density function) which is a scalar function of one of the strain tensors, and whose derivative with respect to one strain component determines the corresponding stress component. This can be expressed by

$$\mathbf{S} = \frac{\partial W}{\partial \mathbf{E}} = 2\frac{\partial W}{\partial \mathbf{C}} \tag{19}$$

where $\mathbf{S}$ is the second Piola-Kirchoff stress tensor. It is noted the definition of W can be multiple for different materials.

Based on the principle of virtual displacement, we have the virtual work:

$$\delta U = \delta\mathbf{u}^T\mathbf{M}\ddot{\mathbf{u}} + \delta\mathbf{u}^T\mathbf{A}\dot{\mathbf{u}} + \int_{V_0}\delta\mathbf{E}^T\mathbf{S}dV - \delta\mathbf{u}^T\mathbf{F}_{ext} - \delta\mathbf{u}^T\mathbf{R} = 0 \tag{20}$$

where $\mathbf{M}$ is the mass matrix, $\mathbf{A}$ the damping matrix, $\mathbf{F}_{ext}$ the vector of external loads, $\mathbf{R}$ the contact reaction vector, $\dot{\mathbf{u}}$ the velocity vector and $\ddot{\mathbf{u}}$ the acceleration vector.

Since $\dot{\mathbf{u}}$ is arbitrary, the non-linear govern equations can be given as:

$$\mathbf{M}\ddot{\mathbf{u}} + \mathbf{A}\dot{\mathbf{u}} + \mathbf{F}_{int} - \mathbf{F}_{ext} - \mathbf{R} = 0\,. \tag{21}$$

where $\mathbf{F}_{\text{int}}$ is the vector of internal forces, which can be defined:

$$\mathbf{F}_{\text{int}} = \int_{V_0}\delta\mathbf{E}^T\mathbf{S}dV \tag{22}$$

Substituting $\delta\mathbf{E}$ from Eq.(17) and $\delta\mathbf{S}$ from Eq.(19) into Eq.(22), we have:

$$\mathbf{F}_{\text{int}} = \int_{V_0} (\mathbf{B}_L + \mathbf{B}_{NL}(\mathbf{u}))^T \frac{\partial W}{\partial \mathbf{E}} dV \tag{23}$$

4 Time step integration and contact solution

The governed equations Eq.(21) for dynamic contact problems can be transformed into:

$$\mathbf{M}\ddot{\mathbf{u}} = \mathbf{F} + \mathbf{R} \tag{24}$$

where

$$\mathbf{F} = \mathbf{F}_{ext} - \mathbf{F}_{int} - \mathbf{A}\dot{\mathbf{u}} \tag{25}$$

The solution to Eq.(24) differs between explicit and implicit approaches. The explicit method [19,28] appears to be efficient, but unstable, and without checking convergence. The implicit method [16,27,29] is supposed to be accurate. However, the computation is much more expensive for large deformation associated to multibody system. To solve these problems, a semi-explicit algorithm is applied in this work.

Let us consider the duration $[t, t + \Delta t]$, Eq.(24) is more convenient to be expressed as:

$$\begin{aligned} &\textstyle\int_t^{t+\Delta t} \mathbf{M} d\dot{\mathbf{u}} = \int_t^{t+\Delta t} \mathbf{F} dt + \int_t^{t+\Delta t} \mathbf{R} dt \\ &\mathbf{u}_{t+\Delta t} = \mathbf{u}_t + \textstyle\int_t^{t+\Delta t} \dot{\mathbf{u}} dt \end{aligned} \tag{26}$$

The initial state at $t = 0$, $\dot{\mathbf{u}}_t = \dot{\mathbf{u}}_0, \mathbf{u}_t = \mathbf{u}_0$.

To evaluate integrals in Eq.(26), we choose the Euler integration scheme:

$$\int_t^{t+\Delta t} \mathbf{M} d\dot{\mathbf{u}} = \mathbf{M}(\dot{\mathbf{u}}_{t+\Delta t} - \dot{\mathbf{u}}_t) \tag{27}$$

$$\int_t^{t+\Delta t} \mathbf{F} dt = \Delta t((\mathbf{F}_{\text{ext}})_{\mathbf{t}} - (\mathbf{F}_{\text{int}})_{\mathbf{t}} - \mathbf{A}\dot{\mathbf{u}}_{\mathbf{t}}) \tag{28}$$

$$\int_t^{t+\Delta t} \mathbf{R} dt = \Delta t \mathbf{R}_{\mathbf{t}+\boldsymbol{\Delta}\mathbf{t}} \tag{29}$$

$$\mathbf{u}_{t+\Delta t} = \mathbf{u}_t + \dot{\mathbf{u}}_{t+\Delta t} \Delta t \tag{30}$$

The stiffness effect is included in Eq.(28) by the internal forces vector:

$$(\mathbf{F}_{\text{int})_t} = \int_{V_0} (\mathbf{B}_L + \mathbf{B}_{NL}(\mathbf{u_t}))^T \frac{\partial W}{\partial \mathbf{E}} dV \tag{31}$$

By applying Eq.(8), the above equations from Eq.(26) to Eq.(29) can result in an implicit relationship between $\dot{\mathbf{u}}_{t+\Delta t}$ and the local contact force $\mathbf{r}_{t+\Delta t}$, such that

$$\dot{\mathbf{u}}_{t+\Delta t} = (\mathbf{M})^{-1}\Delta t((\mathbf{F}_{ext})_t - (\mathbf{F}_{\text{int}})_t + \mathbf{H}^T\mathbf{r}_{t+\Delta t}) + \dot{\mathbf{u}}_t - \Delta t(\mathbf{M})^{-1}\mathbf{A}\dot{\mathbf{u}}_t \tag{32}$$

$\mathbf{M}$ and $\mathbf{A}$ do not change, hence the factorization of the two coefficient matrixes can be computed only once at the beginning.

By submitting Eq.(32) into Eq.(9), we have:

$$\dot{\mathbf{x}} = \mathbf{W}\mathbf{r}_{t+\Delta t} + \mathbf{\Phi} \tag{33}$$

with

$$\begin{aligned} \mathbf{W} &= \mathbf{H}\mathbf{M}^{-1}\Delta t\mathbf{H}^T \\ \mathbf{\Phi} &= \mathbf{H}\mathbf{M}^{-1}\Delta t((\mathbf{F}_{ext})_t - (\mathbf{F}_{\text{int}})_t) + \mathbf{H}\dot{\mathbf{u}}_t - \mathbf{H}\Delta t(\mathbf{M})^{-1}\mathbf{A}\dot{\mathbf{u}}_t \end{aligned} \tag{34}$$

In a reduced local system of equations, for each contact point α, among N_c instantaneous contact points, the relationship between $\dot{\mathbf{x}}^\alpha$ and $\mathbf{r}^\alpha_{\mathbf{t+\Delta t}}$ can be written as:

$$\dot{\mathbf{x}}^\alpha_{t+\Delta t} - \mathbf{W}^{\alpha\alpha}\mathbf{r}^\alpha_{t+\Delta t} = \sum_{\beta=1}^{\alpha-1} \mathbf{W}^{\alpha\beta}\mathbf{r}^\beta_{t+\Delta t} + \sum_{\beta=\alpha+1}^{N_c} \mathbf{W}^{\alpha\beta}\mathbf{r}^\beta_{t+\Delta t} + \mathbf{\Phi}^\alpha \tag{35}$$

where $\mathbf{W}^{\alpha\beta}$ is an influence matrix that takes account of the coupling between contact points α and β. For each contact point α, this equation is solved by considering other contact points ($\alpha \neq \beta$) as "frozen".

4.1 The bi-potential method

De Saxcé and Feng [15] proposed a unique mathematical operator of projection within the bi-potential framework, such that

$$\mathbf{r} = \text{proj}(\mathbf{r}^*, K_\mu) \quad \text{with} \quad \mathbf{r}^* = \mathbf{r} - \rho(\dot{\mathbf{x}}_t + (\dot{x}_n + \mu||\dot{\mathbf{x}}_t||)\mathbf{n}) \tag{36}$$

where $\mathbf{r}^*$ is the so-called augmented contact force vector. $\mathbf{r}$ implies the projection of $\mathbf{r}^*$ onto the closed convex Coulomb's cone. ρ is an positive parameter which is determined by the reduced flexibility matrix.

The three possible contact statuses as mentioned in Eq.(15) thus can be explicitly stated as

$$\begin{aligned}
&\mathrm{Proj}(\mathbf{r}^*, K_\mu)=\mathbf{0} \quad \text{if} \quad \mu\,\|\mathbf{r}_\mathbf{t}^*\| \le -\mathbf{r}_\mathbf{n}^* && \text{separating} \\
&\mathrm{Proj}(\mathbf{r}^*, K_\mu)=\mathbf{r}^* \quad \text{elseif} \quad \|\mathbf{r}_t^*\| \le \mu r_n^* && \text{sticking} \\
&\mathrm{Proj}(\mathbf{r}^*, K_\mu)=\mathbf{r}^* - \left(\tfrac{\|\mathbf{r}_t^*\|-\mu r_n^*}{1+\mu^2}\right)\left(\tfrac{\mathbf{r}_t^*}{\|\mathbf{r}_t^*\|} - \mu\mathbf{n}\right) && \text{sliding}
\end{aligned} \tag{37}$$

Therefore, by applying the projection operation in Eq.(35) and the Eq.(36), solving the contact force leads to the following equations:

$$\mathbf{f}(\chi) = \begin{Bmatrix} \mathbf{f}^1(\chi) \\ \vdots \\ \mathbf{f}^{Nc}(\chi) \end{Bmatrix}, \chi = \begin{Bmatrix} \chi^1 \\ \vdots \\ \chi^{Nc} \end{Bmatrix}, \chi^\alpha = \begin{Bmatrix} \mathbf{r}_{t+\Delta t}^\alpha \\ \dot{\mathbf{x}}_{t+\Delta t}^\alpha \end{Bmatrix} \tag{38}$$

with

$$\mathbf{f}^\alpha(\chi) = \begin{Bmatrix} \dot{\mathbf{x}}_{t+\Delta t}^\alpha - \mathbf{W}^{\alpha\alpha}\mathbf{r}_{t+\Delta t}^\alpha - \dot{\mathbf{x}}^{\alpha\beta}=\mathbf{0} \\ \mathbf{Z}^\alpha = \mathbf{r}_{t+\Delta t}^\alpha - \mathrm{Pr\,oj}(\mathbf{r}_{t+\Delta t}^{*\alpha}, K_\mu) \end{Bmatrix} \tag{39}$$

$$\dot{\mathbf{x}}^{\alpha\beta}=\sum_{\beta=1}^{\alpha-1}\mathbf{W}^{\alpha\beta}\mathbf{r}_{t+\Delta t}^\beta+\sum_{\beta=\alpha+1}^{Nc}\mathbf{W}^{\alpha\beta}\mathbf{r}_{t+\Delta t}^\beta+\mathbf{\Phi}^\alpha \tag{40}$$

4.2 Local solution

For each time step, the numerical solution of Eq.(39) can be performed by an iterative process involving one predictor-corrector step. The process can be stated as follows:

-Step 1: Initiation

$$\begin{Bmatrix} \mathbf{r}_0^\alpha = \mathbf{0} \\ \dot{\mathbf{x}}_0^\alpha = \dot{\mathbf{x}}_k^{\alpha\beta} \end{Bmatrix}, j = 0 \tag{41}$$

-Step 2: Prediction phase

$$\mathbf{r}_{j+1}^\alpha = \mathbf{r}_j^\alpha + \Delta\mathbf{r}_j^\alpha \tag{42}$$

with

$$\Delta\mathbf{r}_j^\alpha = -\rho((\dot{\mathbf{x}}_t)_j^\alpha + ((\dot{x}_n)_j^\alpha + \mu||(\dot{\mathbf{x}}_t)_j^\alpha)||\mathbf{n}) \tag{43}$$

-Step 3: Correction phase

$$\mathbf{r}^{\alpha}_{j+1} = \mathrm{Proj}_{K_\mu}(\mathbf{r}^{\alpha}_{j+1}) \tag{44}$$

-Step 4: Convergence check

$$\begin{aligned} &\text{if} \quad ||\Delta \mathbf{r}^{\alpha}||/\mathbf{r}^{\alpha}_{j+1} > \varepsilon_1 \,\text{then} \\ &\dot{\mathbf{x}}^{\alpha}_{j+1} = \mathbf{W}^{\alpha\alpha}\mathbf{r}^{\alpha}_{j+1} + \dot{\mathbf{x}}^{\alpha\beta}_{k}, j = j+1 \\ &\quad \text{return to step 2} \\ &\text{else} \quad \mathbf{r}^{\alpha}_{k+1} = \mathbf{r}^{\alpha}_{j+1} \end{aligned} \tag{45}$$

where k and $k+1$ are the iteration numbers of the global solution in the Gauss-Seidel algorithm [30]. ε_1 is the user-defined convergence tolerance of the local solution.

The proposed method is conditional stable for non-linear problems. An estimation of time step depends on the characteristic length of the smallest element l:

$$\Delta \mathrm{t} \leq \delta \frac{l}{c_L}, \quad \mathrm{c}_L = \sqrt{\frac{E}{\rho_m}} \tag{46}$$

where c_L is the wave speed, E the young‘s modulus, ρ_m the mass density. The constant δ $0.2 < \delta < 0.9$ is a reduction factor which has to be chosen empirically for the problem.

For the current discussion, the global contact force $\mathbf{R}$ is treated explicitly in views of Eq.(24). Nevertheless, this is not the case for the local contact force $\mathbf{r}$, which is implicitly related to the velocity $\dot{\mathbf{x}}_{t+\Delta t}$, within the bi-potential framework. Consequently, the proposed integration scheme is called semi-explicit. During each iteration step, the hyperelasticity is considered by calculating the internal force at element level, which avoids assembling a stiffness matrix, and when the mass matrix $\mathbf{M}$ and $\mathbf{A}$ are simplified to be diagonal, the system of equations can be solved without factorization. Accordingly, the cost of each iteration can be highly reduced.

5 Methodology for contact detection

5.1 Octrees-based structure for the top stage

The Octree data structure [31,32] is a common technique for the phase of broad detection. It works well to exclude the impossible intersecting objects as well

as identify the likelihood of potential collisions of objects. Normally, Octree represents the 3D volume as a hierarchy of discrete octants, in which each parent octant is recursively subdivided into eight child octants. The Octree structure is searched from the root down to determine collisions. Only objects that share the same octants are taken to have potential contacts.

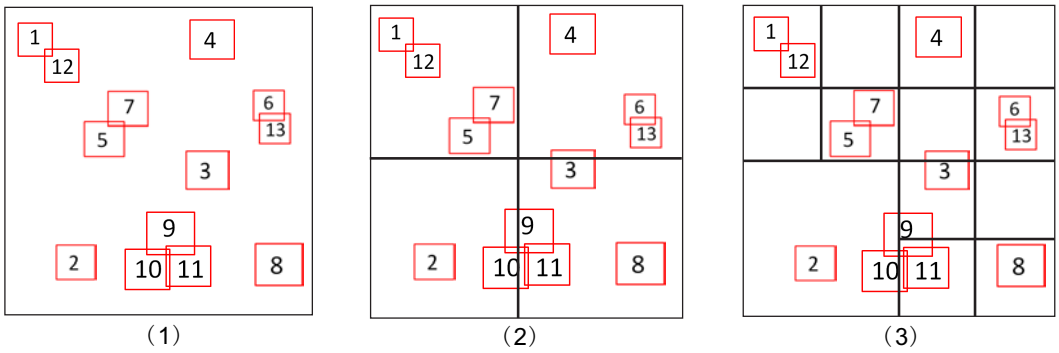

Fig. 2. A 2D example of Octree. (1) represents the root level, (2) and (3) respectively denotes the level 1 and level 2.

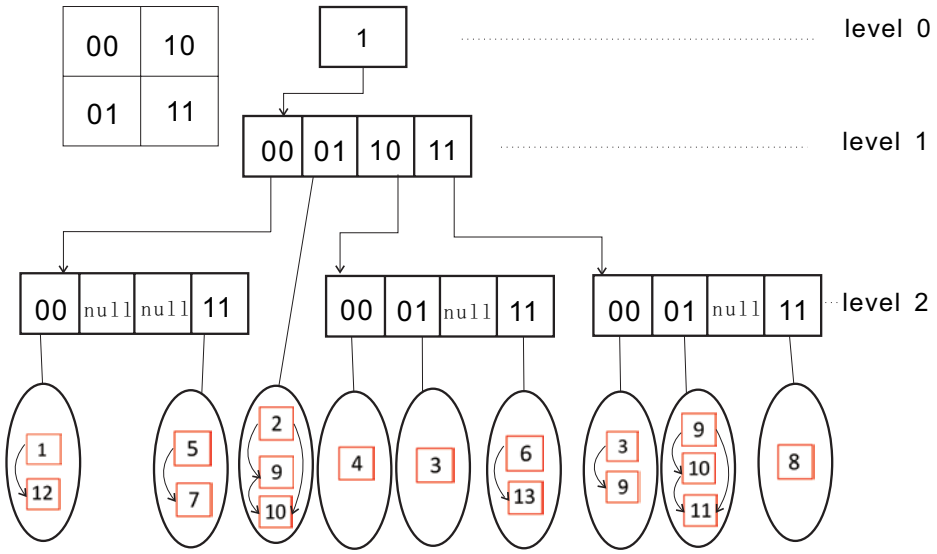

Fig. 3. Schematic of pointer-based Octree structure

We propose an Octree representation as a pointer-based structure, similar to [33]. The octant can be added or removed as required, thus is well suited to dynamic problems that update frequently. An illustrative diagram of 2D equivalent is shown in Figure 2. The corresponding schematic of determination of collisions is shown in Figure 3. Each octant stores pointers to its four children. But only these non-empty octants are considered to take memory, while others are defined *Null*. This allows all the search paths to be tested with a lower memory storage. The position of each octant can be encoded with a binary index from $0-3$. The root octant is assigned as 1, and its

four children octants are denoted as $00, 01, 10, 11$. The recursive location of objects terminates when the branch reaches the tree depth, or the number of objects per octant below the predefined value. Here, the maximum number of objects per octant is predefined as 3, and the depth of the tree as 3. It can be found in Figure 3 that, there are altogether nine non-empty leaf octants, and $1+1+3+1+1+3=10$ potential contact pairs. Compared to brute force method that performs $13*(13-1)/2=78$ broad checks, the Octree structure can significantly reduce the computational cost.

5.2 Bounding volume hierarchy for the middle stage

As mentioned above, a set of potential object-object pairs can be filtered from the first stage. Then, the problem for the middle stage lies on how to detect real local contact areas between an object pair, or more precisely the elementary pairs (e.g. node-segment(2D), node-triangle(3D), node-quad(3D)) between two meshes. For this purpose, the technique of bounding volume hierarchies (BVH) is adopted for primitive queries. Types of bounding volumes (BVs) include spheres, axis-aligned bounding boxes (AABBs), discretely oriented polytopes (K-DOPs), or a hybrid of them. Detailed introductions on bounding volume hierarchies can be found in the book by Ericson [34]. Here we employ the popular AABBs to make a good trade-off between the tightness of fit and the computational cost.

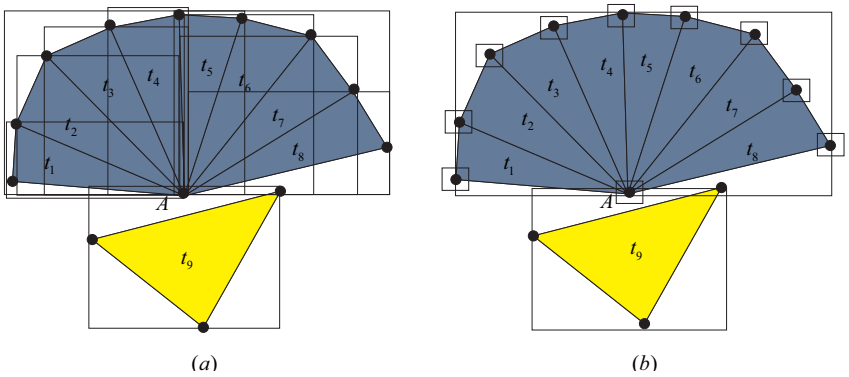

Fig. 4. Elementary test between vertex A and face t_9

Classically, hierarchy-based approaches for the intersection detection between meshes merely use triangle elements as the fundamental primitives. However, this strategy may result in duplicate queries, because exact elementary tests only depend on vertex-triangle pairs rather than triangle-triangle pairs. For example, the vertex A (Figure 4 (a)) is incident to eight triangles (t_1,,,t_8), and A comes into contact with triangle t_9. Culling approaches by simply using triangles will produce eight times triangle-triangle tests, and 24 times vertex-triangle tests. However, only vertex A and triangle t_9 are the pairs to be really

intersected, while all the other elementary tests are false positives. To solve this problem, we propose to create bounding volumes based on specific geometric components, i.e. vertices, edges and faces, see Figure 4 (b). BVs on the surface Ω_1 are directly constructed by a vertex set, while BVs on the surface Ω_2 are created by a triangle set. As a result, the duplications illustrated in Figure 4 (a) could not happen, because each bounding volume enclosed a vertex is represented only once in the hierarchy, thus the overlapping between vertex A and triangle t_9 would be unique. Furthermore, the separated hierarchies can improve the culling efficiency of the elementary testing. Because the volume occupied by a vertex can be much smaller than any other types of geometric component. Also, it is important to note that the simplest linear triangle element can be replaced by other more complicated types in the context of finite element analysis, e.g. 6-node triangle, 4-node quad, 8-node quad, etc.

Algorithm 1 `Elementary searching`

```
1: VBVH represents the vetex-based BVH.
2: TBVH represents the triangle-based BVH.
3: procedure ContactQuery(VBVH, TBVH)
4:     Node1 = Root(VBVH)
5:     Node2 = Root(TBVH)
6:     Traversal (Node1, Node2)
7:     if BV(Node1) and BV(Node2) do not intersect then
8:         Return
9:     end if
10:    if Node1 and Node2 are leaves then
11:        add Node1 − Node2 into elementary pair list
12:    end if
13:    if Node1 is not a leaf then
14:        Traversal (LeftChild(Node1), Node2)
15:        Traversal (RightChild(Node1), Node2)
16:    else
17:        Traversal (Node1, LeftChild(Node2))
18:        Traversal (Node1, RightChild(Node2))
19:    end if
20: end procedure
```

A vertex-based hierarchy or a triangle hierarchy can be built in a typical top-down manner [35], by finding a suitable splitting plane to partition the primitives. To ensure a balanced tree, we position the splitting plane orthogonal to the longest AABB axis, which should pass through the median of the centroid coordinates. Any primitive is classified depending on its location with respect to the splitting plane. Given two meshes, all the contact elementary pairs can be searched by a recursive algorithm, as is stated in the pseudo-code above. The traversal is performed down from the root of BVH, and ends until the leaf node is reached. If the BVs of two nodes do not intersect, it is then

not needed to test the intersection between the children of the two nodes. As a result, this BVH search complexity is in a logarithmic order, which is particularly efficient for cases with very few contact elements, but a very large data system.

5.3 Local contact search for the low stage

When elementary pairs are detected by the tests on bounding volumes of the previous level, a more elaborate resolution is needed to discern whether these pairs are really in penetrated condition. Here, we present a local contact search method based on the iso-parametric space, by which a nearest antagonist point on the contact surface can be determined.

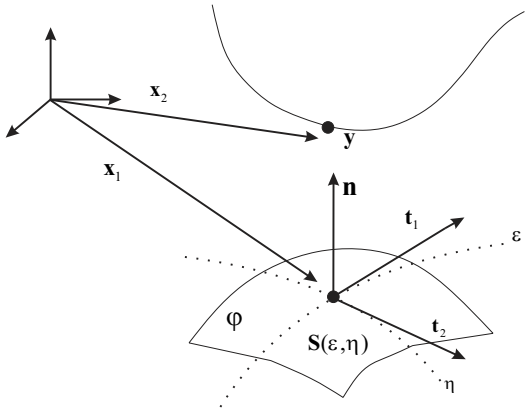

Fig. 5. Contact node location

Consider that a surface φ of the domain has a parametric form $\mathbf{S}(\varepsilon,\eta)$, as shown in Figure 5. Any point on the surface can be presented by $\mathbf{S}(\varepsilon,\eta) = \sum N_i(\varepsilon,\eta)\mathbf{x}_i$, where N_i denotes the Lagrangian shape function associated to the node position $\mathbf{x_i}$. Let point $\mathbf{y}$ be the potential counterpart of the contact surface φ as illustrated in Figure 5, the closest point from φ to $\mathbf{y}$ can be obtained after solving the following system of equations:

$$(\varepsilon^*,\eta^*) = \underset{\xi,\eta}{\operatorname{argmin}}\, H(\varepsilon,\eta) = \frac{1}{2}||\mathbf{S}(\varepsilon,\eta)-\mathbf{y}||^2 \tag{47}$$

Accordingly, Eq.(47) is equivalent to the following vector form:

$$F(\mathbf{X}) = \begin{bmatrix} f_1(\mathbf{X}) = (\mathbf{S}(\varepsilon,\eta)-\mathbf{y})\cdot\mathbf{v}_\varepsilon \\ f_2(\mathbf{X}) = (\mathbf{S}(\varepsilon,\eta)-\mathbf{y})\cdot\mathbf{v}_\eta \end{bmatrix} = 0, \quad \mathbf{X} = \begin{bmatrix} \varepsilon \\ \eta \end{bmatrix} \tag{48}$$

where $\mathbf{v}_\varepsilon = \frac{\partial \mathbf{S}(\varepsilon,\eta)}{\partial \varepsilon}$, $\mathbf{v}_\eta = \frac{\partial \mathbf{S}(\varepsilon,\eta)}{\partial \eta}$.

The problem stated by Eq.(48) may be nonlinear when the surface φ is curved, for example, the quadrilateral face. Thus, the solution can be obtained by the Newton-Raphson iterative process:

$$\begin{cases} \mathbf{X}^0(\text{initial vector}) \\ J(\mathbf{X}^{(k)})(\Delta\mathbf{X}^{(k)}) = F(\mathbf{X}^{(k)}) \\ \mathbf{X}^{(k+1)} = \mathbf{X}^{(k)} - \Delta\mathbf{X}^{(k)} \end{cases} \tag{49}$$

where $J(\mathbf{X}^{(k)}) = \begin{pmatrix} \frac{\partial f_1(\mathbf{X}^{(k)})}{\partial \varepsilon} & \frac{\partial f_1(\mathbf{X}^{(k)})}{\partial \eta} \\ \frac{\partial f_2(\mathbf{X}^{(k)})}{\partial \varepsilon} & \frac{\partial f_2(\mathbf{X}^{(k)})}{\partial \eta} \end{pmatrix}$.

The iterations usually converges in four or less iterations. The final solution (ε^*, η^*) should satisfy the conditions: $-1 \leq \varepsilon^* \leq 1, -1 \leq \eta^* \leq 1$.

6 Numerical examples

The described algorithms above are implemented in the in-house finite element program FER/Impact [36] via $C++$. To illustrate the results of the multibody dynamic simulation, we consider here two numerical examples.

6.1 Dynamic contact between ten 2D hyperelastic cylinders

We firstly consider here one $2D$ example to show the validity of the proposed semi-explicit method. This example concerns altogether ten soft bodies impact onto a concave rigid surface. The initial configuration and finite element meshes are displayed in Figure 6. The radius of the smaller cylinder is 0.14 m, and the the radius of the larger cylinder is 0.28 m. The finite element discretization includes 1318 four-node isoparametric plane strain elements and 1528 nodes. The Blatz-Ko hyperelastic model [37] is adopted here, with the material parameters: shear modulus $G = 2 \times 10^6$ Pa, mass density $\rho = 800$ kg/m^3, friction coefficient $\mu = 0.2$, and initial velocity $v_x = 0$ m/s, $v_y = -20$ m/s. The total simulation time is 0.07 s, and the time step is $\Delta t = 10^{-5}$ s.

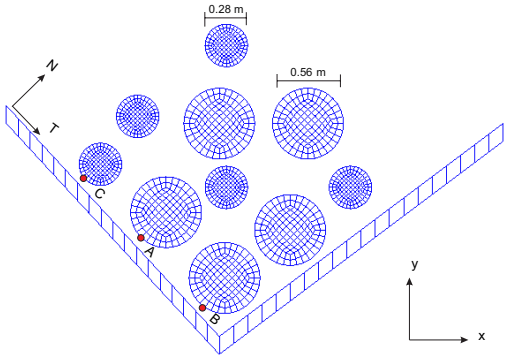

Fig. 6. Initial geometry of mesh

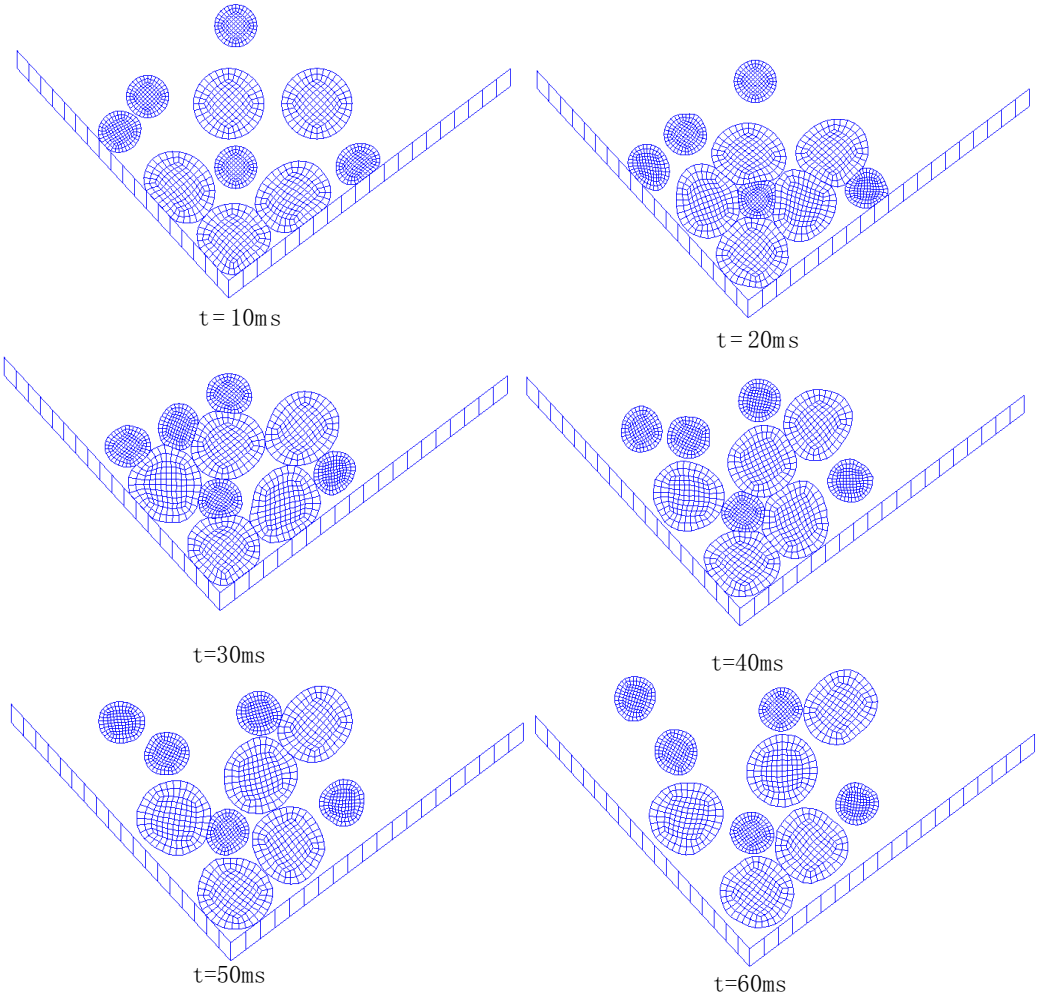

Fig. 7. Deformed shape during the process

Figure 7 shows the evolution of deformed shapes at different time steps. Figure 15 plots the displacements u_N of three selected nodes (A, B, C) versus time. u_N is along the local N direction (see Figure 6) and also perpendicular to the

left rigid surface. The results demonstrate that our approach allows to satisfy accurately the contact impenetrability condition.

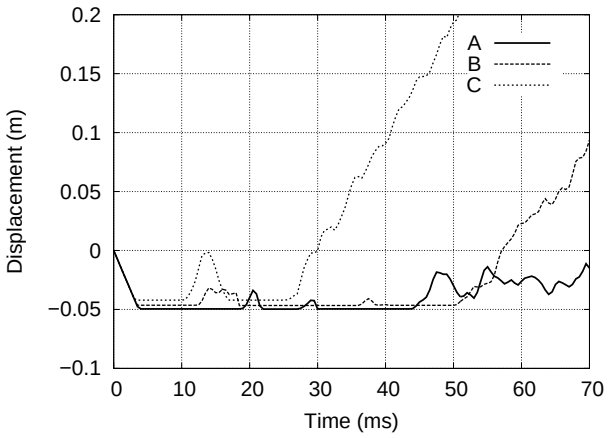

Fig. 8. Displacements of nodes

For the purpose of comparison, we use the implicit scheme developed by Feng et al [16] for analysis of the same problem. The implicit integration parameters are chosen as $\theta = 0.5$, $\xi = 0.5$. In Figure 9, the distribution of von Mises stress is performed at time $t = 20.5$ ms. We observe that, the achieving maximum value of von Mises stress (5.767×10^6 Pa) by semi-explicit scheme is slightly lower than the result (6.112×10^6 Pa) obtained from implicit scheme.

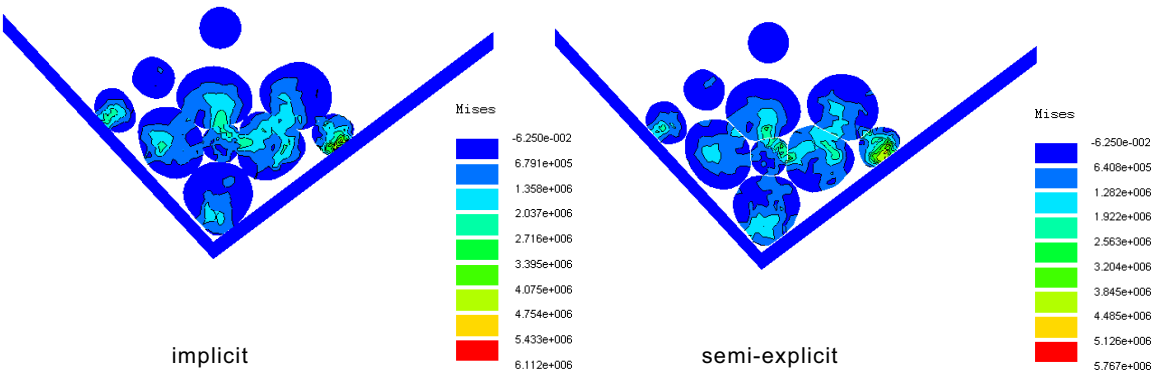

Fig. 9. Distribution of von Mises stress at time $t = 20.5ms$

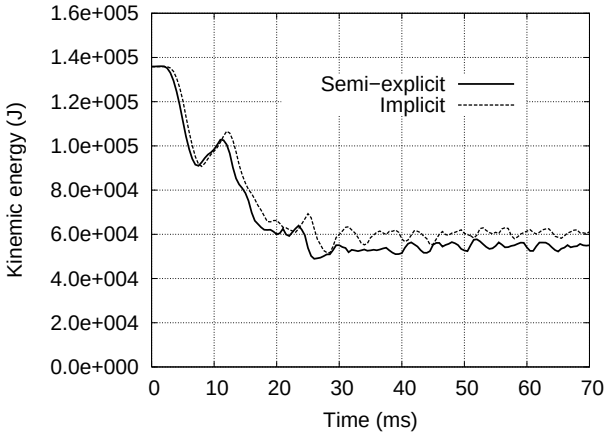

Fig. 10. Comparison between semi-explicit and implicit scheme: kinetic energy

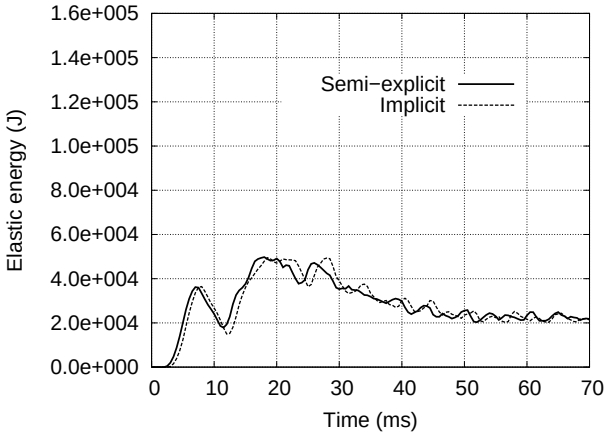

Fig. 11. Comparison between semi-explicit and implicit scheme: elastic energy

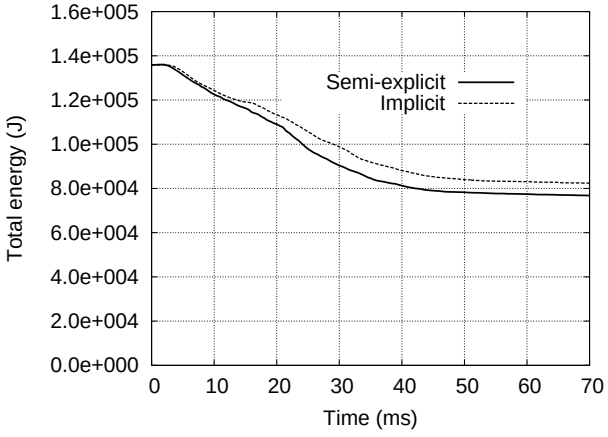

Fig. 12. Comparison between semi-explicit and implicit scheme: total energy

Figure 12-11 show respectively the plots of the kinetic energy E_k, the elastic strain energy E_e, and the total energy $E_t = E_k + E_e$ as a function of time. We can note that the results by the semi-explicit scheme can be as accurate and

stable as the implicit scheme. But in Table 1, the total computational time by the semi-explicit scheme is significantly lower (almost ten times) as compared to the implicit scheme. The results in Table 1 also indicate that the solution for semi-explicit algorithm may become divergent when time step is large, for example $\Delta t = 1e^{-3}s$. It is noted that the simulation was performed on a PC (i5-5200U 2.20 GHz).

Table 1
Comparison of CPU time

Δt (s)	$1e^{-3}$	$1e^{-4}$	$1e^{-5}$	$1e^{-6}$
semi-explicit (s)	divergence	38.22	349.62	3978.37
implicit (s)	50.25	398.52	3682.18	41210.45

6.2 Dynamic contact between 3D hyperelastic bodies

The second example aims to illustrate the frictional effects and the efficiency of the proposed contact detection algorithm. First of all, 25 hyperelastic cubes are modeled to impact with a rigid plate, see Figure 13. The length of the smaller cube is 0.5 m, and the length of the larger one is 0.55 m. The total finite element discretization consists of 1608 nodes and 676 hexahedron 8-node elements. Here, we once again apply the non-linear Blatz-Ko model. The material characteristics are: shear modulus $G = 2 \times 10^7$ Pa, mass density $\rho = 800\,\mathrm{kg/m^3}$. The velocity is $\{0.0, -20.0, -10.0\}$ (m/s). The total processing time is 0.05 s and the time step is : $\Delta t = 0.0001$ s. We assume that no damping exists. The coefficients of Coulomb friction for different cases are defined: $\mu = 0.0$(frictionless), 0.5.

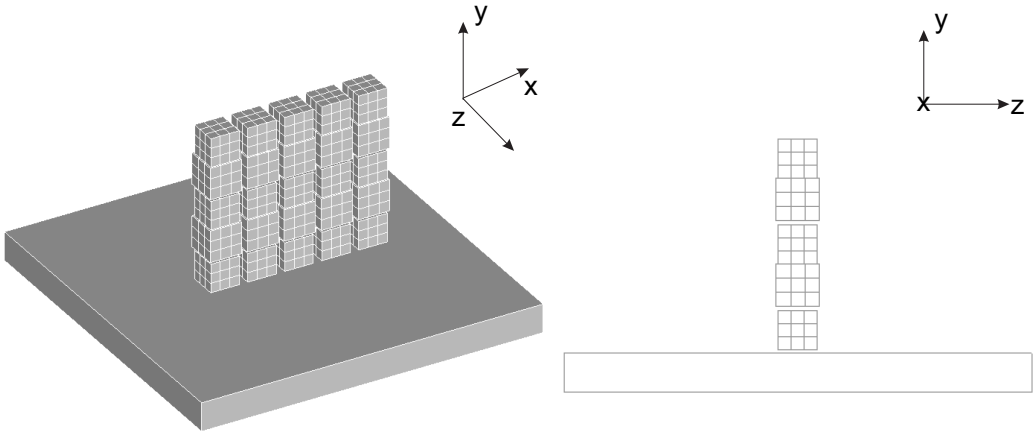

Fig. 13. Initial configurations and meshes

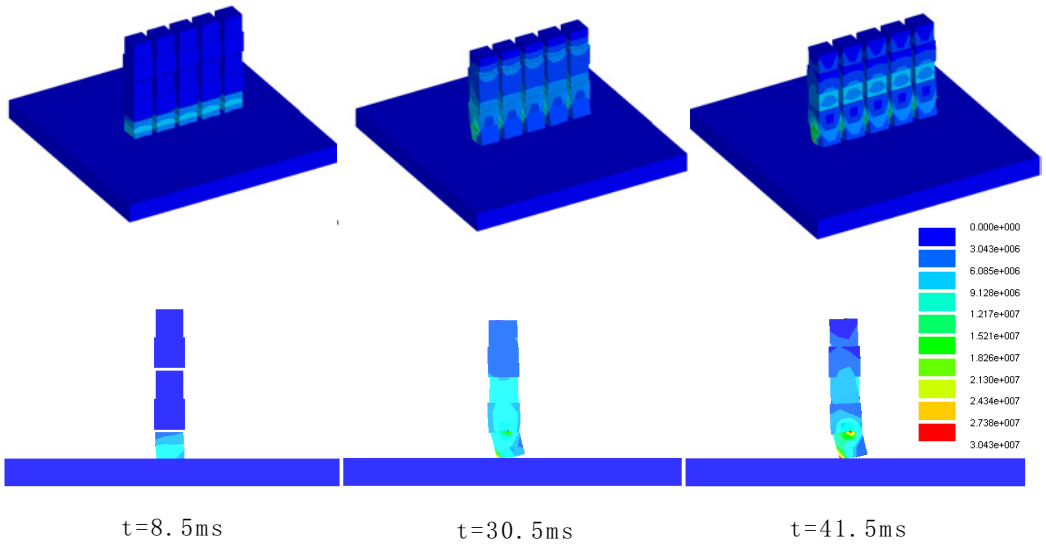

Fig. 14. Deformed shape and von-Mises stress ($\mu = 0.5$)

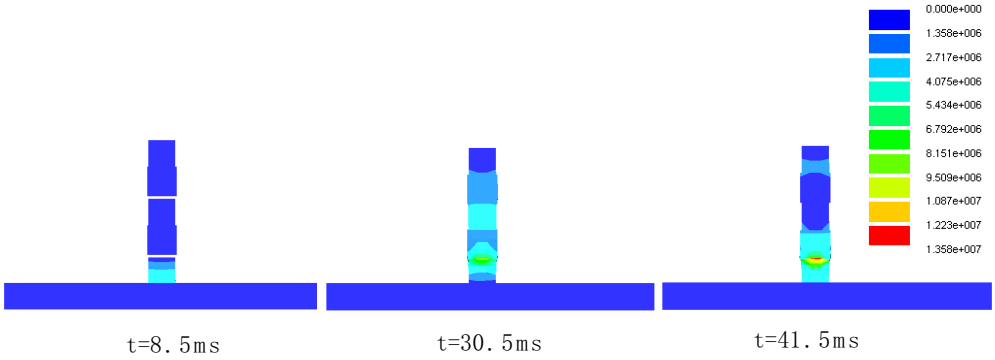

Fig. 15. Deformed shape and von-Mises stress ($\mu = 0.0$)

Figure 14 shows the evolution of von-Mises stress at three time instants $t = 8.5$ ms, $t = 30.5$ ms, $t = 41.5$ ms. The isocontours presents the maximum value of von-Mises stress at the left bottom and the middle upward side of the lowest cube ($\mu = 0.5$). It is noted that the undersurface does not completely cling to the base surface. However, this is not the case for $\mu = 0.0$, see Figure 15. We can also observe that the distribution of von-Mises stress is symmetrical to y direction when no friction is applied. The frictional effects are so apparently demonstrated.

Table 2 shows the elementary pairs, the contact search time and the total computational time versus the time step. At each time step, we note that the cost for contact detection only takes a very small part of the total computational time. For the purpose of comparison, we analyze the same example by a brute force method and a classical BVH method, see Table 3. The proposed optimal BVH can be ten times faster than the classical BVH, and almost 700 times faster than the brute force method.

Table 2
Computational time along time steps

$t(s)$	$elementary-pairs$	$search-time$ (s)	$total-time$ (s)
0	160	0.015	0.141
0.010	240	0.017	0.265
0.020	250	0.017	0.266
0.030	320	0.028	0.406
0.040	330	0.031	0.391
0.050	190	0.017	0.203

Table 3
Search time for 500 steps

$methods$	$search-time$ (s)	$total-time$ (s)	$percentage$
brute force	7720.023	7867.056	0.9813
classic BVH	124.234	277.020	0.4484
optimal BVH	11.662	167.626	0.0695

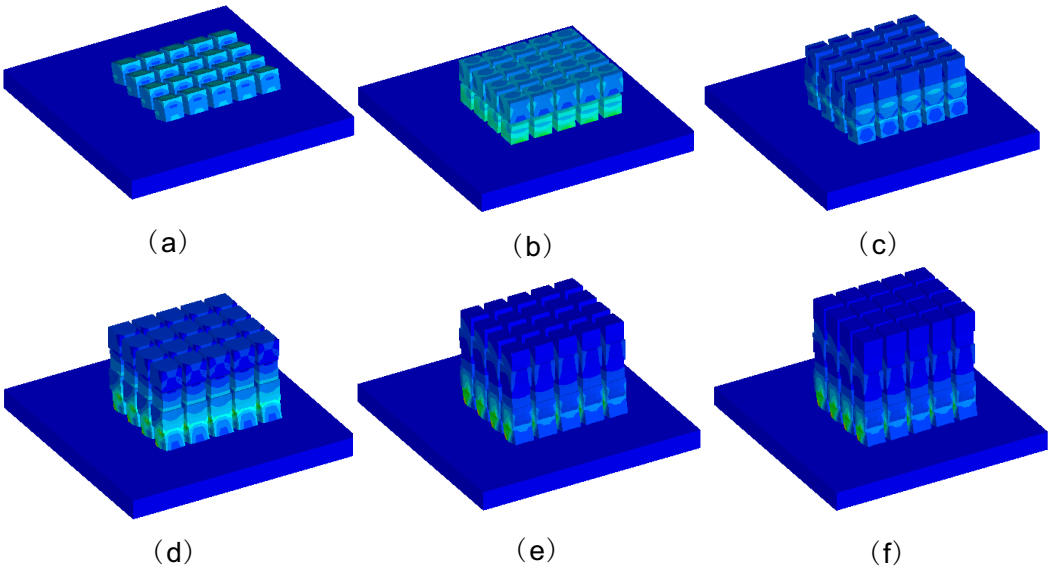

Fig. 16. Impact with different number of cubes. Each cube has 56 contact nodes and 54 contact quads on the surface. (a) 20 cubes with 1120 contact nodes, (b) 40 cubes with 2240 contact nodes, (c) 60 cubes with 3360 contact nodes, (d) 80 cubes with 4480 contact nodes, (e) 100 cubes with 5600 contact nodes, (f) 120 cubes with 6720 contact nodes.

As is demonstrated in Table 3, the contact search by using a unsuitable method

can easily dominate (> half) the CPU time required for simulation. Thus, a problem arises: if the proposed contact detection methodology would become inefficient with increasing problem sizes? To investigate this issue, we perform another example by gradually increasing the number of cubes impacting on the rigid plate, see Figure 16. The material and integration parameters remain the same as the second $3D$ example. Figure 17 plots the total computational time on the contact detection algorithm as a function of the numbers of contact nodes for 500 time steps. The results indicate that the contact searching time by using the proposed algorithms does not fit a linear relation with the contact nodes. This is because both the Octree and BVH require a logarithmic search complexity. In Figure 18, we can find that the rate of the contact detection time with respect to the total computation time decreases when contact nodes increase, which is opposite to the tendency in Figure 17. Therefore, the applicability of the proposed methodology in dealing with multibody contact problems with a large data system can be confirmed.

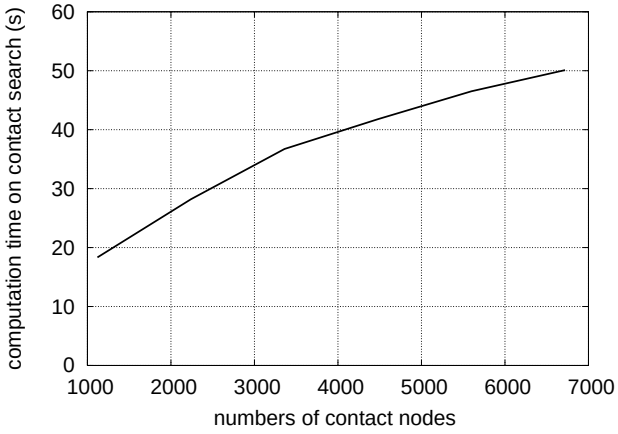

Fig. 17. Computation time on contact searching for 500 time steps

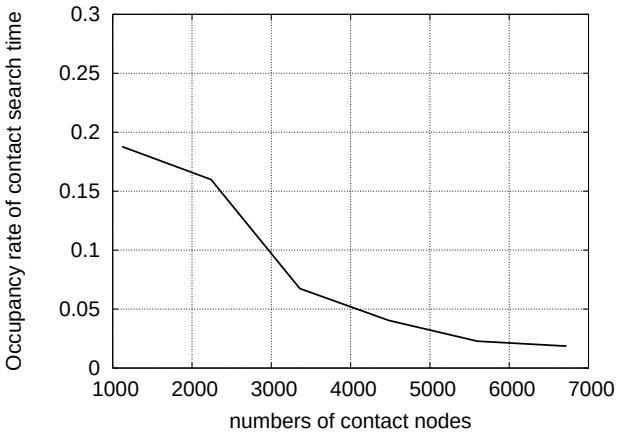

Fig. 18. Occupancy rate of contact searching time with respect to total computation time

7 Concluding remarks

This paper presents a semi-explicit algorithm to solve the multibody dynamics with friction and large deformation. Taking the implicit integration scheme as a reference, the results obtained by the semi-explicit algorithm confirm its good accuracy and stability in deal with high frequency multibody dynamics. However, for larger time steps, the solution may become divergent. The results show also that the proposed algorithm is fast in terms of computational time for systems with a large number of degrees of freedom and complex nonlinearities.

To accelerate the contact detection for multibody systems, a hybrid three stages methodology is then proposed. In particular, an optimal bounding volume hierarchy is used to detect elementary pairs, which can significantly reduce the duplicate tests. In general, this contact search method can also be applied to deal with self-contact problems when some modifications are made. The presented work can also be extended to solve contact problems with millions of degrees of freedoms by using parallel computation.

Acknowledgement

We gratefully acknowledge the financial support of the National Key R&D Program of China (Grant No. 2017YFB0703200) and the National Natural Science Foundation of China (Grant No. 11772274).

References

[1] R. K. Misra, A. Dixit, and H. S. Mali. Finite element (FE) shear modeling of woven fabric textile composite. *Procedia Materials Science*, 6:1344–1350, 2014.

[2] Y. Bei and B. J. Fregly. Multibody dynamic simulation of knee contact mechanics. *Medical Engineering & Physics*, 26:777–789, 2004.

[3] Y. C. Lin, J. P. Walter, S. A. Banks, M. G. Pandy, and B. G. Fregly. Simultaneous prediction of muscle and contact forces in the knee during gait. *Journal of Biomechanics*, 43:945–952, 2010.

[4] S. W. Kim. *Contact dynamics and force control of flexible multi-body systems*. PhD thesis, McGill University Libraries, 1999.

[5] K. Yoshida, N. Sashida, R. Kurazume, and Y.Umetani. Modeling of collision dynamics for space free-floating links with extended generalized inertia tensor.

In *Proceedings of the 1992 IEEE International Conference on Robotics and Automation*, pages 889–904. IEEE, 1992.

[6] Y. Wang and M. Mason. Modeling impact dynamics for robotic operations. In *Proceedings of the 1987 IEEE International Conference on Robotics and Automation.*, pages 678–685. IEEE, 1987.

[7] R. M. Brach. Formulation of rigid body impact problems using generalized coefficients. *International Journal of Engineering Science*, 36:61–71, 1998.

[8] Billy. Fredriksson. Finite element solution of surface nonlinearities in structural mechanics with special emphasis to contact and fracture mechanics problems. *Computers & Structures*, 6:281–290, 1976.

[9] S.K. Chan and I. S. Tuba. A finite element method for contact problems of solid bodies. *International Journal of Mechanical Sciences*, 13:615–625, 1971.

[10] Y. Kanto and G. Yagawa. A dynamic contact buckling analysis by the penalty finite element method. *International Journal for Numerical Methods in Engineering*, 29:755–774, 1990.

[11] P. Alart and A. Curnier. A mixed formulation for frictional contact problems prone to newton like solution methods. *Computer Methods in Applied Mechanics and Engineering*, 92:353–375, 1991.

[12] J. C. Simo and T. A. Laursen. An augmented lagrangian treatment of contact problems involving friction. *Computers & Structures*, 42:97–116, 1992.

[13] K. J. Bathe and A. Chaudhary. A solution method for planar and axisymmetric contact problems. *International Journal for Numerical Methods in Engineering*, 21:64–88, 1985.

[14] R. L. Taylor and P. Papadopoulos. On a finite element method for dynamic contact/impact problems. *International Journal for Numerical Methods in Engineering*, 36:2123–2140, 1993.

[15] G. De Saxcé and Z.-Q. Feng. The bipotential method: a constructive approach to design the complete contact law with friction and improved numerical algorithms. *Mathematical and Computer Modelling*, 28:225–245, 1998.

[16] Z. Q. Feng, P. Joli, J. M. Cros, and B. Magnain. The bi-potential method applied to the modeling of dynamic problems with friction. *Computational Mechanics*, 36:375–383, 2005.

[17] Z.-Q. Feng, F. Peyraut, and Q.-C. He. Finite deformations of Ogden's materials under impact loading. *International Journal of Non-Linear Mechanics*, 41:575–585, 2006.

[18] J. O. Hallquist, G. J. Goudreau, and D. G. Benson. Sliding interfaces with contact-impact in large-scale lagrangian computations. *Computer Methods in Applied Mechanics and Engineering*, 51:107–137, 1985.

[19] D. J. Benson and J. O. Hallquist. A single surface contact algorithm for the post-buckling analysis of shell structures. *Computer Methods in Applied Mechanics and Engineering*, 78:141–163, 1990.

[20] S. Gottschalk, M. C. Lin, and D. Manocha. I-COLLIDE: An interactive and exact collision detection system for large-scale environments. In *Proceedings of the 1995 symposium on Interactive 3D graphics*, pages 189–196. ACM, 1995.

[21] E. G. Gilbert, D. W. Johnson, and S. S. Keerthi. A fast procedure for computing the distance between complex objects in three-dimensional space. *IEEE Journal of Robotics and Automation*, 4:193–203, 1988.

[22] S. Cameron. Enhancing GJK: Computing minimum and penetration distances between convex polyhedra. In *ICRA*, pages 20–25. Citeseer, 1997.

[23] M. C. Lin and J. F. Canny. A fast algorithm for incremental distance calculation. In *IEEE International Conference on Robotics and Automation*, pages 1008–1014. IEEE, 1991.

[24] H. Chen, Z. Lei, and M. Zang. LC-Grid: a linear global contact search algorithm for finite element analysis. *Computational Mechanics*, 54:1285–1301, 2014.

[25] P. Jiménez, F. Thomas, and C. Torras. 3D collision detection: a survey. *Computers & Graphics*, 25:269–285, 2001.

[26] M. Lin and S. Gottschalk. Collision detection between geometric models: A survey. In *Proceedings of IMA conference on mathematics of surfaces*, pages 602–608. IMA, 1998.

[27] T. A. Laursen and J. C. Simo. A continuum-based finite element formulation for the implicit solution of multibody, large deformation-frictional contact problems. *International Journal for Numerical Methods in Engineering*, 36:3451–348, 1993.

[28] T. Belytschko and M. O. Neal. Contact-impact by the pinball algorithm with penalty and lagrangian methods. *International Journal for Numerical Methods in Engineering*, 31:547–572, 1991.

[29] J. J. Mareau. Unilateral contact and dry friction in finite freedom dynamics. In *Nonsmooth Mechanics and Applications*, pages 1–82. Springer, 1988.

[30] F. Jourdan, P. Alart, and M. Jean. A Gauss-Seidel like algorithm to solve frictional contact problems. *Computer Methods in Applied Mechanics and Engineering*, 155:31–47, 1998.

[31] D. J. Kim, L. J. Guibas, and S. Y. Shin. Fast collision detection among multiple moving spheres. *IEEE Transactions on Visualization and Computer Graphics*, 4:230–242, 1998.

[32] B. C. Vemuri, Y. Cao, and L. Chen. Fast collision detection algorithms with applications to particle flow. In *Computer Graphics Forum*, pages 121–134. Wiley Online Library, 1998.

[33] J. Wilhelms and A. V. Gelder. Octrees for faster isosurface generation. *ACM Transactions on Graphics (TOG)*, 11:201–227, 1992.

[34] Christer. Ericson. *Real-time Collision Detection*. CRC Press, 2004.

[35] G. Bergen. Efficient collision detection of complex deformable models using AABB trees. *Journal of Graphics Tools*, 4:1–13, 1997.

[36] Z.-Q. Feng. http://lmee.univ-evry.fr/∼feng/FerImpact.html.

[37] P.J. Blatz and W.L. Ko. Application of finite elastic theory to the deformation of rubbery materials. *Transactions of the Society of Rheology*, 6:223–251, 1962.

A semi-explicit algorithm for solving multibody contact dynamics with large deformation
L. Peng, Z.Q. Feng, P. Joli
Submitted to the International Journal of Non-linear Mechanics.

Highlights

- An efficient semi-explicit algorithm is developed to solve the multibody contact dynamics.
- The unilateral contact constraints are enforced via a reaction-velocity formulation within the framework of bi-potential.
- A hybrid methodology consisting of the Octree structure and the bounding volume hierarchy is proposed to reduce exhaustive contact inspections.